

Progress and Future Prospects for Particle-Based Simulation of Hypersonic Flow

Thomas E. Schwartzentruer*

*Department of Aerospace Engineering and Mechanics
University of Minnesota, Minneapolis, MN, 55455*

and

Iain D. Boyd†

*Department of Aerospace Engineering
University of Michigan, Ann Arbor, MI, 48109*

The direct simulation Monte Carlo method (DSMC) has evolved over 50 years into a powerful numerical technique for the computation of thermochemical nonequilibrium gas flows. In this context, nonequilibrium means that velocity and internal energy distribution functions are not in equilibrium forms due to a low number of intermolecular collisions within a fluid element. In hypersonic flow, nonequilibrium conditions occur at high altitude and in regions of flow fields with small length scales. This article highlights significant developments in particle simulation methods (since 2001) applied specifically to hypersonic flows, which now includes Molecular Dynamics in addition to DSMC. Experimental measurements that have led directly to improved DSMC models will be highlighted. Algorithm development for DSMC aimed at increasing computational efficiency is discussed with a focus on hybrid particle-continuum methods. New research that applies all-atom Molecular Dynamics simulation and trajectory-based DSMC simulation to normal shock waves is summarized. Finally, a discussion of state-resolved DSMC modeling is included with reference to future prospects for particle simulation methods and in particular for the DSMC method.

I. Introduction

When modeling gases in nonequilibrium, the atomistic/molecular nature of the gas must be explicitly accounted for. This is especially true for gases in thermochemical nonequilibrium which involve finite-rate translational-rotational-vibrational-electronic relaxation as well as chemical reactions. Such finite rate processes, when coupled with low densities, small length-scales, high gradient regions, or high flow speeds, can result in strong thermochemical nonequilibrium in the bulk flow and next to vehicle surfaces. Understanding and prediction of the precise thermochemical gas state within the flow field surrounding a vehicle and within the boundary layer next to a vehicle's surface is crucial in order to design hypersonic flight vehicles and thermal protection systems. Particle simulation methods have proven to be a valuable tool for fundamental understanding and design of hypersonic systems and have enormous potential as computational power continues to rapidly increase.

Since changes in the state of a dilute gas occur via molecular collisions, the relevant spatial scale is the mean free path (λ) and the relevant temporal scale is the mean collision time (τ_c). Below this temporal scale, $O(\tau_c)$, no variations in the gas state are possible and likewise, no changes are possible below a spatial scale of $O(\lambda)$. Furthermore, in a dilute gas there are an enormous number of molecules within a volume of λ^3 , ranging from tens-of-thousands at sea level to billions (per λ^3 volume) at altitudes typical of hypersonic flight. It is unnecessary to account for the properties of all real molecules, rather, their local distribution

*Email address: schwartz@aem.umn.edu

†Email address: iainboyd@umich.edu

functions (for velocity, internal energy, chemical species, etc.) are sufficient to completely describe the nonequilibrium state of the gas. Such distribution functions can be accurately constructed by considering only a small fraction of the real molecules. In addition, the pre-collision orientations (the impact parameters) of colliding molecules are completely random in a dilute gas. The direct simulation Monte Carlo (DSMC) method takes advantage of these three inherent properties of dilute gases by using simulator particles that each represent a large number of identical real molecules, moving simulator particles with timesteps on the order of τ_c , and stochastically selecting collision pairs and initial orientations within volumes (computational cells) on the order of λ . These are rigorous simplifications based on sound physical principles. Present DSMC methods then go one step further and use probabilistic rules to determine the local collision rate and collision outcomes, thus introducing collision *models*.

The DSMC method was first introduced by Graeme Bird in 1961.¹ Since that time, Bird has written two books on the method^{2,3} and thousands of research papers have been published that report on development and application of the technique. The significance of the DSMC technique has been its ability over 50 years of development to provide a method of analysis for high Knudsen number flows (conditions ranging from continuum to free-molecular). Strong nonequilibrium in a flow is characterized by large Knudsen numbers ($Kn = \lambda/L > 0.01$), where L is a characteristic length of interest in the flow. A DSMC simulation emulates the same physics as the Boltzmann equation. In fact, it has been demonstrated that DSMC converges to solution of the Boltzmann equation in the limit of a very large number of particles.³ For low Knudsen numbers ($Kn = \lambda/L < 0.01$), through Chapman-Enskog theory,⁴ the Boltzmann equation reduces exactly to the Navier-Stokes equations, which are the governing equations for computational fluid dynamics (CFD) simulations. Therefore, DSMC and CFD methods provide a highly consistent modeling capability for gas flows spanning the entire Kn range. DSMC collision models are extremely flexible in that they can be phenomenological and formulated to be consistent with continuum thermochemical rate data or they can directly incorporate ab initio quantum chemistry results. This flexibility in physical modeling enables DSMC to provide high fidelity calculations of multispecies gases in strong thermochemical nonequilibrium over full vehicle geometries. For example, DSMC has been used recently to support the Columbia Space Shuttle orbiter accident investigation,⁵ to support the 2001 Mars Odyssey aerobraking mission,⁶ and to analyze the post-flight data from the Stardust mission.⁷⁻¹⁰ The utility of DSMC and its range of applications continues to expand in-step with advances in computational resources.

This article focuses on particle simulation methods applied to hypersonic flows. The long term goals in this field involve (i) large-scale particle simulations that completely overlap with CFD simulations for complex 3D flows (this involves research into computational efficiency and ultimately hybrid DSMC-CFD capability), (ii) advancing phenomenological (reduced-order) models for engineering design and analysis, and (iii) incorporating ab initio based (quantum chemistry) collision models directly into particle simulations to improve our understanding of hypersonic flows at the most fundamental level. As with any numerical modeling approach, these advancements must be validated by experimental data and should also aid in the design of new experiments required to move the science forward.

II. Experimental Validation

In this section, a review is provided of the status of the application of the DSMC technique to hypersonic flows. We first consider the application of DSMC to analyze hypersonic experiments conducted in ground-based facilities. Generation of rarefied, hypersonic flows in ground-based facilities presents a technical challenge, and very few data sets exist that enable a detailed assessment of DSMC codes.

In 2001, a code validation exercise (for both DSMC and CFD) was focused on hypersonic viscous interactions that can be generated on slender body configurations. A series of experiments were performed in the LENS facility for a number of configurations including double cones, and cylinder-flares.¹¹ While several groups performed DSMC analyses of some of these cases, Moss and Bird¹² provide the most comprehensive comparisons with the measured data. Figure 1 shows comparisons for surface pressure and heat flux for a Mach 15.6, $Kn=0.001$ flow of nitrogen over a double cone configuration. DSMC results from two different codes (DS2V and SMILE) are provided and clearly give excellent agreement with the measurements. Similar levels of agreement between DS2V DSMC computations and measurements of pressure and heat flux are also shown in Ref. 13 for a Mach 12.4, $Kn=0.0004$ flow of nitrogen over a cylinder flare configuration. For these flows, the vibrational energy of nitrogen was barely activated, and thus there was no chemistry present under these conditions.

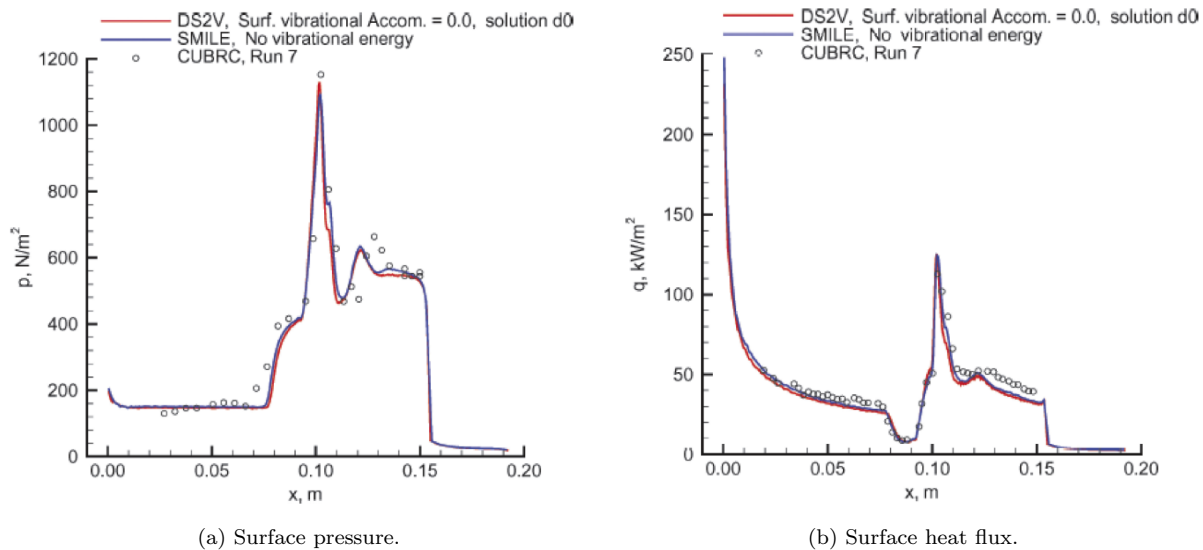


Figure 1: Measured versus computed surface properties for a double cone geometry tested with nitrogen at Mach 15.6, $Kn=0.002$.¹³

The Bow-Shock Ultra-Violet-2 (BSUV-2) hypersonic flight experiment (a slender vehicle geometry) was flown in 1991.¹² The vehicle geometry consisted of a spherically-capped 15 deg. cone with a nose radius of about 10 cm. BSUV-2 reentered the atmosphere at 5.1 km/sec and provided data in the altitude range from 110 to 60 km. Measurements of the ultra-violet emission due to nitric oxide and vacuum-ultra-violet emission due to atomic oxygen resonance transitions were obtained by on-board instrumentation. Calculation of the radiative emission was performed in a decoupled approach. The chemically reacting flow field was computed using both continuum (CFD)^{14–16} and particle (DSMC) methods.¹⁷ Then, the emission was predicted from the flow field solutions using the NASA nonequilibrium radiation code NEQAIR.¹⁸ Initial comparisons between DSMC-based results and measurement produced poor agreement at high altitude. This led to significant activity in the study of the oxygen dissociation and nitric oxide formation chemistry models used in the DSMC computations.^{17,19} The final results obtained for nitric oxide radiance as a function of altitude are shown in Fig. 2a.²⁰ Note that the BSUV-2 Knudsen number ranged from 0.008 at 71 km to 0.215 at 90 km. In addition to obtaining very good agreement with radiance, the spectral features were also reproduced extremely well in the computations as demonstrated in Fig. 2b and the effect of varying the accommodation coefficient (α) is also shown. Good agreement was also obtained between DSMC-based prediction and measurement for atomic oxygen emission. The BSUV-2 studies clearly illustrated that access to detailed experimental measurements are needed in order to make significant advances in thermochemical modeling using the DSMC technique.

The Radio Attenuation Measurement (RAM) experiments involved a series of hypersonic entry flights designed to study communications blackout. This is an important operational issue for all hypersonic vehicles in which the plasma formed at very high speed interferes with radio waves sent to and from the vehicle. The vehicle of interest here (RAM-C II), consisted of a cone with a spherical nose cap of radius 0.1524 m, a cone angle of 9 deg., and a total length of about 1.3 m. While entering at orbital velocity (7.8 km/s), the RAM-C II experiment made measurements from about 90 km to 60 km altitude. Electron number density was measured using two different diagnostics at several locations in the plasma layer surrounding the vehicle.^{21,22} A series of reflectometers was used to measure the maximum plasma density along lines normal to the vehicle surface in four different locations. A rake of Langmuir probes measured variation in the plasma density across the plasma layer near the rear of the vehicle. DSMC analysis of the RAM-C experiment at 81 km was performed by Boyd²³ in order to make assessment of DSMC procedures for simulating charged species (electrons, ions) in trace amounts. The DSMC results were compared directly with the measurements of plasma density taken on the RAM-C II flight and these are shown in Fig. 3. In each case, the sensitivity of

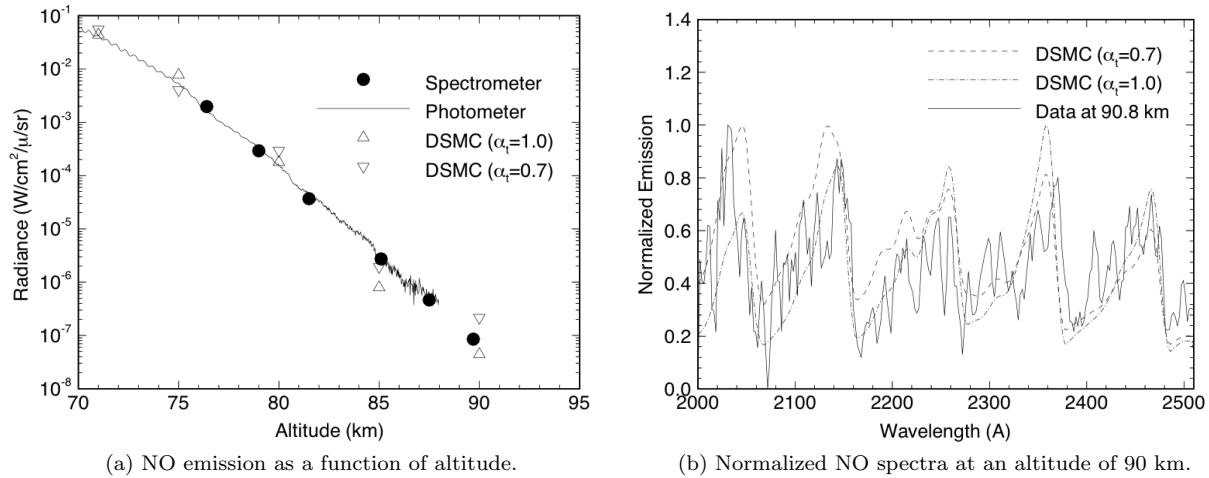


Figure 2: BSUV-2 data and computation comparison.²⁰

the DSMC results to the model employed for dissociation chemistry is investigated. The two models tested were the Total Collision Energy (TCE) model and the Vibrationally Favored Dissociation (VFD) model. Clearly, very good agreement is obtained between simulation and measurement providing validation of the new DSMC procedures.

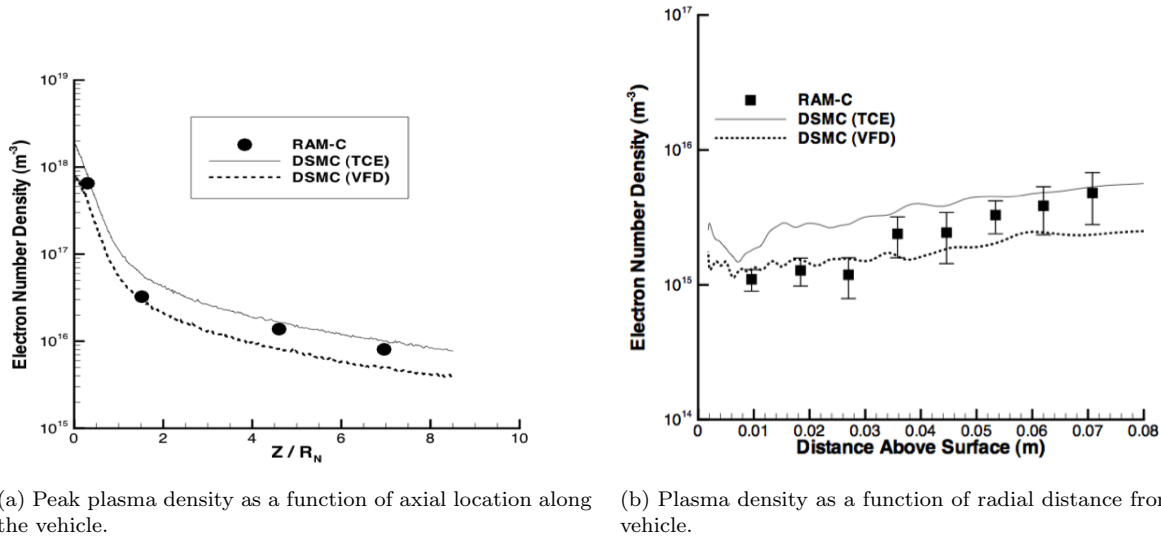


Figure 3: RAM-C II data and computation comparison.²³

Generating high quality experimental data sets in the rarefied hypersonic flow regime continues to be a significant challenge for DSMC development. In order to make optimal use of available resources and experimental facilities, DSMC researchers should help design and propose experiments that will advance the science of nonequilibrium flows.

III. DSMC Algorithm Development

A. Computational efficiency

In general, the computational cost of a DSMC simulation scales linearly with the number of total simulation particles and the number of timesteps required to obtain the solution. Thus any strategy that can reduce the number of particles and/or the number of timesteps while maintaining full accuracy can result in large efficiency gains. Even if each computational cell is precisely adapted to the local value of λ , the number of particles per cell (N_p) will vary with changes in flow density ($\Delta N_p \propto \Delta(1/\rho)$ for 2D flows and $\Delta N_p \propto \Delta(1/\rho^2)$ for 3D flows). Also, for axisymmetric flows, N_p is low near the axis and can be very large far from the axis. An ideal calculation only employs enough particles per cell to obtain statistical accuracy (no more) and would maintain $N_p = \text{const}$ at this value.

A number of efficiency strategies for DSMC were detailed by Kannenberg and Boyd.²⁴ One technique that helps reduce the number of simulation timesteps and also control/reduce N_p is local, cell-based, time-stepping for steady-state flows. Here, ray-tracing is used to move particles through the grid one cell at a time, however each cell has a different timestep associated with it that is adapted to the local mean-collision-time (τ_c). Specifically, each cell stores the value $\Delta t_{ratio} = \tau_c / \Delta t_{ref}$, where Δt_{ref} is a global reference timestep (typically set based on the free stream value of τ_c). Then for each ray-trace movement of Δt , particles are instead moved for $\Delta t_{ratio} \times \Delta t$. The larger the timestep used to move particles through a given cell, the fewer simulation particles will be found in that cell. In order to simulate the correct number density, all particles within the cell are given a particle weight of $W_p = \Delta t_{ratio} \times W_{p-ref}$. This technique achieves, approximately, $N_p = \text{const}$ for 2D flows and $\Delta N_p \propto \Delta(1/\rho)$ for 3D flows without the need to clone or delete simulation particles and with minimal change to the standard DSMC algorithm.

General particle weighting schemes are required to precisely control N_p for 3D flows and also for flows involving trace species. Here simulation particles are deleted or cloned in order to obtain the desired N_p . Cloning can lead to random walk errors. Also, collisions between particles of different weights (i.e. different species) conserves mass, momentum, and energy only on average, which can also lead to random walk errors.² Various strategies are in use to mitigate these effects, such as holding cloned particles within buffers instead of injecting into the simulation simultaneously. However, to date, no elegant and generally accurate solution to particle weighting has been found.

In terms of reducing the number of required computational cells and therefore the total number of particles, LeBeau et al.²⁵ developed the virtual sub-cell (VSC) scheme and Bird²⁶ developed the transient adaptive sub-cell (TASC) scheme. Both schemes seek to lower the mean-collision-separation (MCS) between selected collision pairs which are no longer selected at random within the computational cell. Thus, the cell size can increase to some degree while still maintaining a low MCS. The VSC scheme performs a nearest-neighbor search to select collision partners, while the TASC subdivides each cell into a number of subcells that are used only during the collision algorithm to sort collision pairs in order to minimize the MCS. In order to prevent the same pair from undergoing repeated collisions, it is necessary to keep a record of the last collision partner and, if the last collision partner is chosen again, to exclude this particle and to choose the next-nearest particle instead. Furthermore, since the collision rate is computed within each cell (not within each subcell), then there is limit on the increase in cell size practically achieved by these schemes, before the assumption of a constant collision rate within a large cell leads to simulation inaccuracy.

Burt et al.²⁷ recently introduced an interpolation scheme for the collision rate within computational cells combined with the techniques above. The interpolation scheme was shown to enable an increase in cell size while maintaining full accuracy; a very promising result. It is noted, however, that the series of simulations in which the cell size was varied all used the same particle weight ($W_p = \text{const}$), and thus the same total number of particles. Thus as cell size was increased, the number of particles per cell also increased, and the interpolation scheme was used within each cell. Although the results are very promising, ideally, accuracy could be demonstrated when the number of particles per cell is kept constant, so that using larger cells would reduce the overall number of particles.

Finally, Bird has recently proposed more substantial algorithm modifications²⁸ to the DSMC method with the same goals of reducing the number of timesteps and total particles. Like the schemes above, the MCS is minimized in the proposed algorithms but now particles store their own timestep. This enables the overall simulation to iterate with very small timesteps and particles are only moved when the global time “catches up” with their timestep. Thus only a small fraction of particles are moved during a global timestep iteration. Complete details as well as a rigorous convergence study for 1D Fourier flow can be found in Ref.

29. The new algorithms produced a factor of 2 speedup for Fourier flow simulations compared to standard DSMC algorithms. It was noted that forming nearest-neighbor collision pairs *after* particles have moved for large timesteps is physically inconsistent and leads to inaccuracy in the simulation.²⁹ Also, inaccuracies were noted when a constant collision rate was applied to large cells (as noted above). The new algorithms are promising and future analysis on a hypersonic flow with large density gradients should be performed. Also, since the new algorithms use a small global timestep, a parallel scaling study should be performed. Typically, increasing the communication (more frequent timesteps) and lowering the computational load per partition (only a fraction of particles move and collide per global timestep) would negatively affect parallel scalability.

B. Hybrid DSMC-CFD simulations

A limitation of the DSMC method is that it becomes computationally expensive in the continuum regime due to correspondingly small molecular spatial and temporal scales, which must be resolved to $O(\lambda)$ and $O(\tau_c)$, respectively. However, under such continuum conditions, the Navier-Stokes (NS) equations accurately model the flow and can be solved efficiently. For this reason, various researchers have proposed hybrid numerical methods that adaptively reposition particle and continuum computational domains within a single hybrid simulation and couple particle and continuum regions by transferring information across an interface.^{30–35} A more detailed overview of the various methods that have been proposed can be found in Ref. 36 and Ref. 37. This article will focus on the continued development of the Modular Particle Continuum (MPC) hybrid approach³⁶ which was initially developed by the authors to simulate steady-state hypersonic flows. The MPC method was initially developed and tested for 1-D normal shock waves³⁸ as well as for hypersonic flow over a 2D-cylinder geometry.³⁶ It has since been applied to blunt body flows,^{39,40} shock interaction flows,⁴¹ reentry flows using reaction control jets,⁴² and has been extended to model rotational nonequilibrium,⁴³ vibrational nonequilibrium,⁴⁴ and multi-species flows.⁴⁵ The MPC algorithm loosely couples DSMC and NS regions, which have different mesh densities and are updated using different timesteps.

Such an approach enables both spatial- and temporal-scale decoupling while lending itself to a modular implementation,⁴⁶ which uses existing state-of-the-art DSMC and NS codes (with little modification) within the hybrid code. In general, MPC simulations are able to accurately reproduce full DSMC simulations to the level of velocity and energy distribution functions using less computational resources.

An important study, completed in 2009, relevant to hybrid method development, was performed by Holman and Boyd⁴⁷ who rigorously compared DSMC and CFD solutions for hypersonic flow over cylinders and spheres for a wide range of Mach numbers and Knudsen numbers. Two important aspects of this study were that sufficient computational resources were used to fully resolve all DSMC simulations and that all physical models were formulated consistently between DSMC and CFD. Specifically, the viscosity, thermal conductivity, rotational relaxation, and vibrational relaxation models used by both DSMC and CFD were ensured to be mathematically consistent in the near-equilibrium limit. Sample results from this study⁴⁷ are displayed in Tables 1 and 2, where the agreement between DSMC and CFD predictions for integrated drag and peak heat flux for Mach 10 air flow over a cylinder is summarized for a range of Knudsen numbers. The agreement between DSMC and CFD predictions clearly improved as the Knudsen number decreases and very close agreement was found between DSMC and CFD for a low Knudsen number of 0.002. Such consistency is crucial for any hybrid DSMC-CFD implementation since information must be transferred across DSMC-CFD interfaces in near-equilibrium regions of the flow. As will be elaborated upon later in this section, even subtle inconsistencies in physical models can introduce noticeable error into a hybrid simulation.

Most recently, Deschenes and Boyd implemented the same consistent physical models into the MPC hybrid code and extended its capabilities to flows in rotational⁴³ and vibrational⁴⁴ nonequilibrium. The MPC method starts with a Navier-Stokes solution to the flow problem and evaluates a measure of continuum breakdown within each computational cell by computing the local gradient-length Knudsen number, defined

Kn_∞	DSMC	CFD, no slip	CFD, slip
0.002	29.02	28.93 (−0.39%)	28.91 (−0.31%)
0.01	6.42	6.60 (2.78%)	6.47 (0.79%)
0.05	1.60	1.83 (14.04%)	1.61 (0.14%)
0.25	0.40	0.71 (76.69%)	0.43 (6.39%)

Table 1: Integrated drag [Newtons] and percent difference from DSMC (%).

Kn_∞	DSMC	CFD, no slip	CFD, slip
0.002	1.09×10^5	1.15×10^5 (5.18%)	1.12×10^5 (2.72%)
0.01	4.71×10^4	5.27×10^4 (11.89%)	5.07×10^4 (7.68%)
0.05	2.11×10^4	2.54×10^4 (20.68%)	2.28×10^4 (8.06%)
0.25	6.43×10^3	1.02×10^4 (58.23%)	7.16×10^3 (11.42%)

Table 2: Peak heating [W/m^2] and percent difference from DSMC (%).

as:

$$Kn_{GL-Q} = \lambda \left| \frac{\Delta Q}{Q} \right|, \quad (1)$$

where Q is a macroscopic flow parameter and λ is evaluated in terms of continuum parameters (viscosity and density). Cells in which the computed value of $Kn_{GL-Q} > 0.05$ are flagged as particle regions, thus defining an interface between particle and continuum regions. An example of the initial particle and continuum regions for an MPC simulation of hypersonic nitrogen flow over a cylinder (Mach 15 flow with a free-stream temperature of 217.5K and a wall temperature of 1000 K, with a diameter based $Kn=0.01$) is shown in Fig. 4a where the bow shock wave, boundary layer, and near wake regions are initialized as particle regions. As depicted schematically in Fig. 4b the particle region is extended further into the continuum region by a multiple of λ in order to set up an “overlap region”, where both CFD and DSMC methods compute a solution. Boundary conditions are then imposed on both DSMC and CFD domains using Dirichlet (state-based) conditions. Specifically, DSMC boundary (buffer) cells are continually refreshed with particles sampled from Chapman-Enskog velocity distributions and Boltzmann rotational and vibrational energy distributions corresponding to the local CFD state vector and cell-centered gradients from the corresponding location in the continuum domain. Macroscopic state variables are sampled within DSMC cells next to the interface and are used to prescribe the state within CFD boundary cells (“ghost cells”) that are used to calculate inviscid and viscous fluxes to update the solution within the continuum domain.

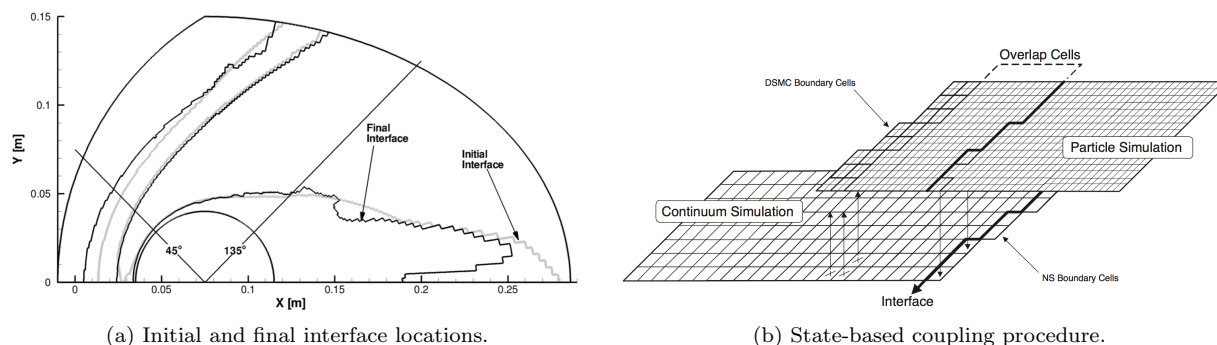


Figure 4: Modular Particle Continuum (MPC) simulation schematic.

The specific application of the MPC method to hypersonic flows typically results in high flow speeds near particle-continuum interfaces ($|\vec{V}| > 10$ m/s for example) and the application to steady-state flows enables loose coupling where boundary conditions do not need to be updated at each timestep. These two results enable any statistical scatter involved in information transfer from DSMC regions to CFD regions to be strictly controlled with simple averaging techniques.⁴⁸ For hypersonic steady-state flows with no trace species, statistical scatter is generally not a limiting factor for hybrid DSMC-CFD simulations, however, further research will be necessary for chemically reacting flows involving trace species.

In contrast, the coupling method between DSMC and CFD regions (for example, *when* to transfer information) requires special consideration in order to obtain accurate hybrid solutions. The basic requirement is that before any information is transferred from the DSMC region to the CFD region, the interface location must be verified to lie in a near-equilibrium region where both DSMC and CFD solutions are expected to agree. If the interface lies in a nonequilibrium region then the CFD boundary conditions will be imposed as a macroscopic average of nonequilibrium distributions; a state (or flux) that the Navier-Stokes equations are not able to handle accurately. The typical result is for the CFD solution to diverge from the correct solution and subsequently provide incorrect boundary conditions for the DSMC region, thereby making the situation worse (see Fig. 5 in Ref. 36 for example).

Instead, as the DSMC solution in the particle region and overlap region evolves, flow gradients (nonequilibrium flow) may enter the overlap region. The solution in the overlap region (initialized as a region where $Kn_{GL-Q} < 0.05$) can be continually monitored for values of $Kn_{GL-Q} > 0.05$. If found, the particle-continuum interface should be extended to encompass these regions and the overlap region extended further by a multiple of λ as discussed above. Thus, the overlap region is essential in that it enables the adaptation of particle-continuum interfaces and can be monitored to ensure that the interface (the location where DSMC

information is transferred to CFD) is indeed in a near-equilibrium region of the solution before transferring any information. In this manner, CFD and DSMC regions can be loosely coupled and the global solution will proceed to a new steady state at which point the interface regions will cease to move and can be locked in place. Afterwards, DSMC and CFD regions continue to be loosely coupled but now cumulative sampling can be used in the DSMC region (since steady state has been reached) enabling the DSMC scatter and therefore the scatter in CFD boundary conditions to be driven to a very low value. This in-turn allows the residual in CFD regions to be driven to equally low values.

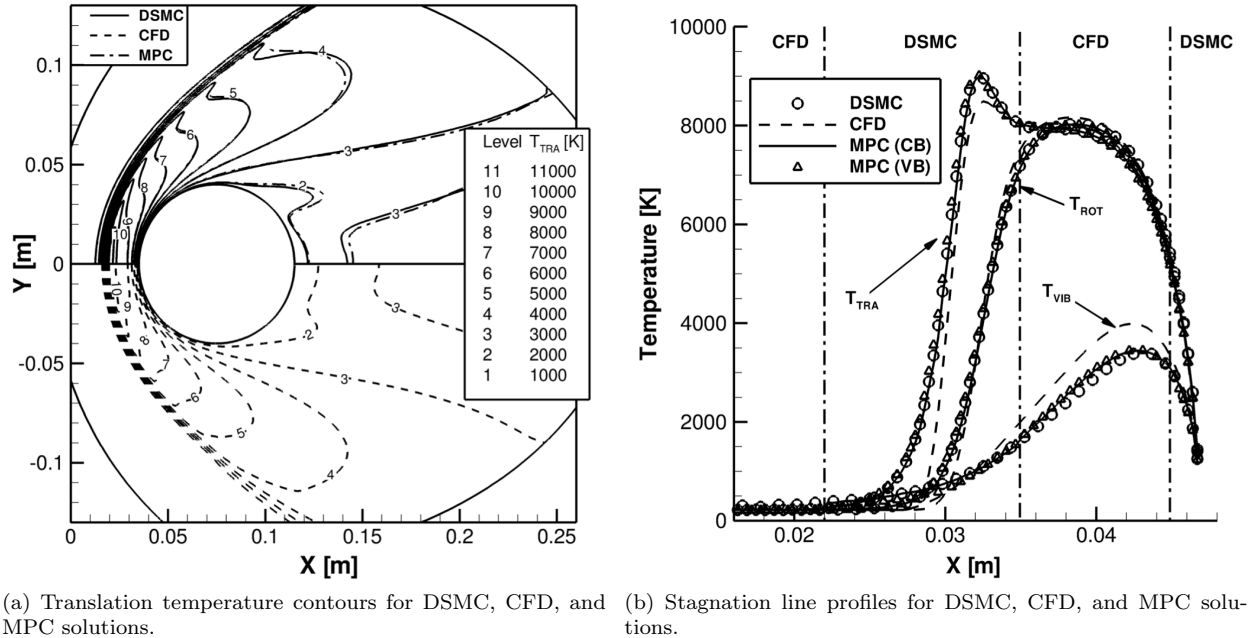


Figure 5: Hybrid DSMC-CFD solutions for hypersonic flow over a cylinder.⁴⁴

The MPC method has undergone continual development since 2007 and most recently has been extended to flows in strong vibrational nonequilibrium by Deschenes and Boyd.⁴⁴ Figure 5a shows the solution for translational temperature for pure CFD, pure DSMC, and MPC calculations for hypersonic flow over a cylinder. The initial and final particle-continuum interface locations were shown earlier in Fig. 4a and the flow conditions were discussed above for this simulation. The MPC solution, initialized to the CFD solution, evolves into very close agreement with pure DSMC while using only a fraction of the particles. Figure 5b shows the properties along the stagnation line predicted by all three methods. It is evident that the CFD simulation predicts steeper gradients in the shock layer than MPC and DSMC (which are in excellent agreement). Also evident in Fig. 5b is that the vibrational temperature profile in the post-shock continuum region (where the MPC method is solving the NS equations) has shifted into excellent agreement with pure DSMC. This demonstrates how a hybrid code can successfully transfer information from isolated nonequilibrium regions and correctly alter continuum portions of the flow.

One interesting result of this study was the influence on the hybrid solution due to a subtle change in the vibrational energy relaxation model. Specifically, the DSMC model was implemented to be consistent with the Launder-Teller expression with a temperature dependent vibrational relaxation rate from Millikan and White.⁴⁹ If the DSMC model is based on the cell-based (CB) temperature, then the DSMC model can be shown to analytically match the continuum model in the equilibrium limit. However, models dependent only on collision properties (not cell averaged properties) are preferred in DSMC since velocity and energy distributions can be highly nonequilibrium. Thus a second DSMC model was tested, herein referred to as the velocity-based (VB) model. The VB model does not have an analytical limit that precisely matches the Launder-Teller equation with a Millikan and White relaxation constant. This is a subtle, but important, issue with many DSMC models that has been investigated in a number of articles.⁵⁰⁻⁵³ Since most continuum thermochemical rate models are curve-fits to experimental data, there is no guarantee that the integration of a physics-based molecular model has the same functional form as the empirical fitting function used for the

continuum model. Thus, perfect consistency in the continuum limit is not always possible between existing DSMC and CFD model formulations. Indeed, future research will require the formulation of new models that are consistent at the molecular and continuum levels and also with experimental data. Figure 6 shows the difference between MPC simulations performed with both vibrational models. When the VB model is used, a discontinuity in the vibrational temperature gradient is seen at the particle-continuum interface (Fig. 6a), whereas when the CB model is used, the temperature gradient varies smoothly across the interface (Fig. 6b).

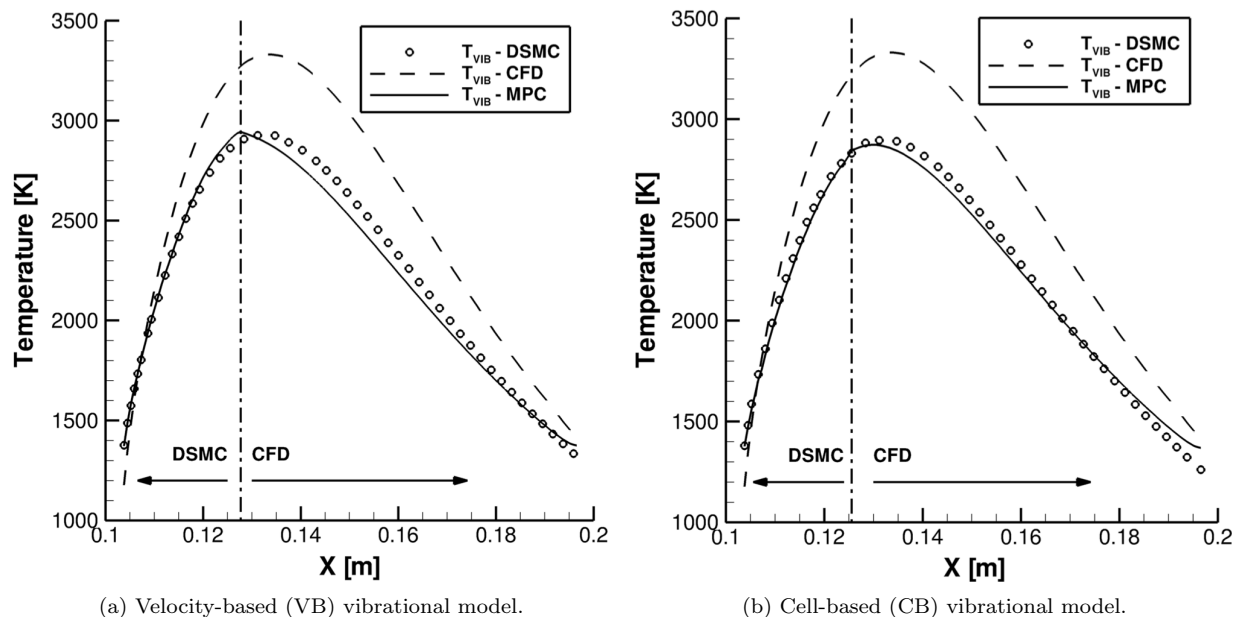


Figure 6: Temperature profiles extracted along the 135 degree line shown in Fig. 4a

In summary, the capabilities of hybrid DSMC-CFD simulations have progressed dramatically in recent years and now include the modeling of flows in strong thermal nonequilibrium (rotation and vibration). Research is proceeding on multispecies flows and flows involving chemistry, where precise consistency between DSMC and CFD models will become even more important and statistical scatter associated with trace species will need to be addressed.

IV. Molecular Dynamics and Trajectory-Based DSMC

All-atom, Molecular Dynamics (MD) simulation of nonequilibrium flow features is now possible through large scale computation. Such high fidelity calculations can be used to develop a fundamental understanding of thermochemical nonequilibrium flows and also to develop reduced-order models for use in DSMC and CFD. Recently, MD studies were performed for normal shock waves in dilute gases.⁵⁴⁻⁵⁷ The sole model input to such MD calculations is a Potential Energy Surface (PES) or a set of PES, which describe the interaction forces between atoms. All atoms in the real system are simulated and the PES are used to integrate atomic motion with femtosecond (10^{-15} s) timesteps. The timestep is typically constrained to be a fraction of the vibrational frequency of any molecules in the system in order to resolve the motion of individual atoms when bound within a molecule. Thus in such MD simulations there are no viscosity, diffusion, or thermal conductivity models and no rotational, vibrational, chemical relaxation rates or state-resolved cross-sections are required. The simulations track the positions and velocities of all individual atoms deterministically and properties such as rotational and vibrational energies of molecules are only post-processed from atom positions and velocities, thus no decoupling of rotational/vibrational energy is assumed within the simulations.

MD simulations were first validated for normal shock waves in dilute argon⁵⁴ with experimental data for shock thickness and with well-established DSMC results. Next, MD simulations were validated with

an extensive experimental data set for argon-helium and xenon-helium mixtures.^{58,59} The agreement with experiment and consistency with DSMC solutions employing both VHS and GHS collision models was very good, as expected.⁵⁶ This particular study demonstrated that resolving low species concentrations (1.5% Xe by mole fraction in one case) is computationally feasible with moderate computational resources and that MD solutions are indeed precise enough to discern the relative accuracy of various DSMC models down to the level of the velocity distribution functions. As an example, the mixture shock simulations required approximately 1 week of continuous run time on 100 core-CPU.

One of the main reasons that pure MD calculations of dilute gases are computationally expensive is that the mean collision time can be much larger than the required femtosecond timesteps and much of the simulation is wasted integrating atomic motion between collisions (free-flight). To address, this, it was further demonstrated that such MD simulations could be greatly accelerated using a combined Event-Driven/Time-Driven algorithm⁵⁵ where atoms are moved directly to their next impending collision, however, an arbitrary PES is used to integrate the collisions. One of the main developments was that in contrast to hard-sphere Event-Driven MD, the algorithm successfully detects and properly integrates multi-body collisions. The resulting EDTD-MD method is purely deterministic and was shown to exactly reproduce pure MD results for argon shock waves in a fraction (proportional to $\Delta t_{MD}/\tau_c$) of the computational time.

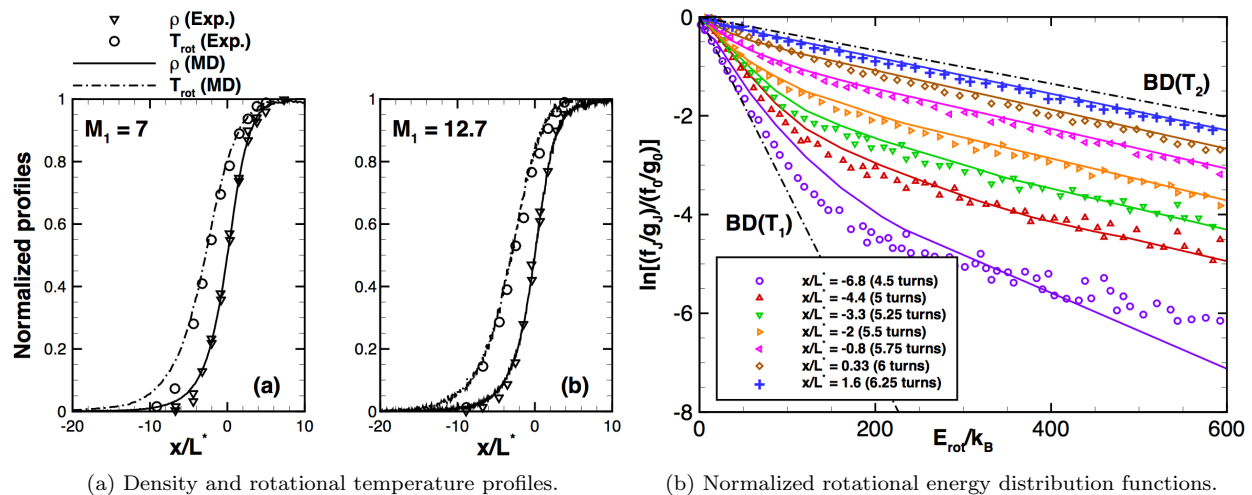
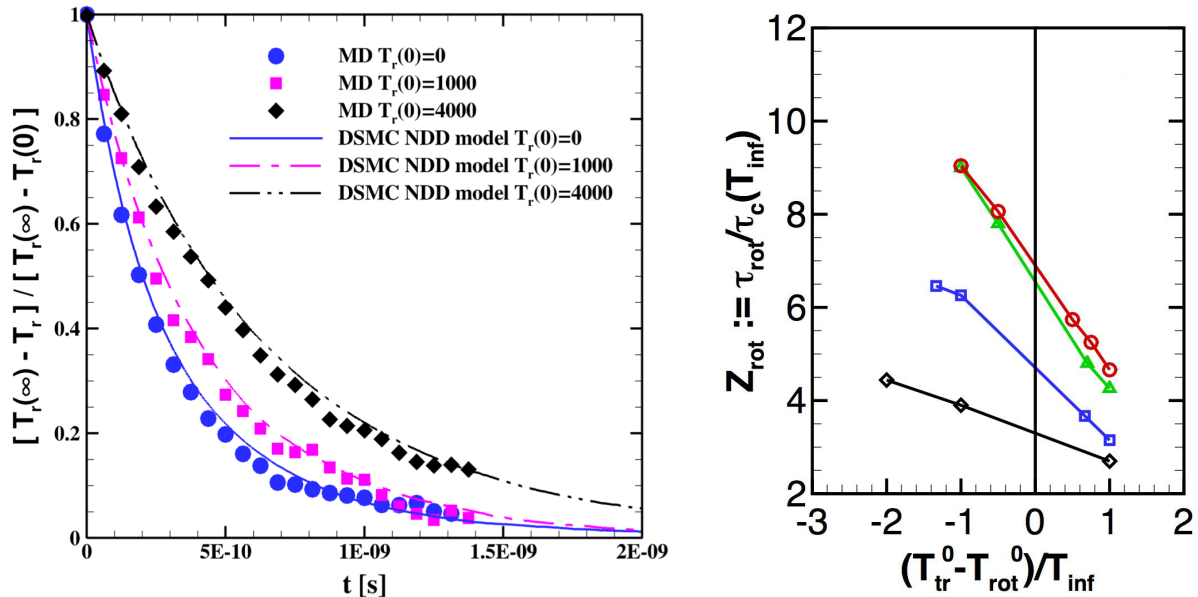


Figure 7: Comparison between MD simulation and experiment for diatomic nitrogen shock waves.⁵⁷

In a subsequent study, all-atom MD simulations of diatomic nitrogen shock waves, expansions, and zero-dimensional relaxations quantified the rotational relaxation rate dependence on the initial direction and deviation from the equilibrium state. This dependence had been speculated in previous papers (for example see Ref. 52), but no experiment or first-principles calculations had resolved this issue. The MD calculations used a site-to-site Lennard-Jones (LJ) model which was first validated with viscosity data and the shock wave experimental data from Robben and Talbot.⁶⁰ For example in Fig. 7a the density and rotational temperature profiles are shown, and in Fig. 7b the rotational distribution functions through the shock are shown.

A number of shock wave, expansion, and relaxation calculations were then performed which clearly showed a dependence of the rotational relaxation rate due to the direction towards equilibrium and also the magnitude of the deviation from the equilibrium state. DSMC and multi-temperature CFD models do not account for such dependence, but rather model the rotational relaxation rate as a function of only the translational temperature (an example is the model by Parker⁶¹). In fact, the MD calculations predicted that the directional dependence is a significantly more dominant effect than the translational gas temperature. For example, three isothermal relaxation (i.e. constant translational temperature equal to the equilibrium temperature) simulations were performed starting with different rotational temperatures. The results are shown in Fig. 8a where different relaxation rates are evident despite the fact that the translational and equilibrium temperatures are the same. Complete MD results for all relaxation calculations, and the dependence of the rotational collision number on both T_{tr} and T_{rot} are shown in Fig. 8b. Clearly, in compressing flows

($T_{tr} > T_{rot}$) rotational excitation is fast (small Z_{rot}), whereas in expanding flows ($T_{tr} < T_{rot}$) rotational de-excitation is slow (large Z_{rot}). Based on this new quantitative data, a simple reduced-order model for DSMC and CFD calculations was developed, called the Nonequilibrium Direction Dependent (NDD) model.⁵³ A single parameterization of the NDD model was able to reproduce available experimental data and all MD solutions for shocks, expansions, and relaxations, in nitrogen.



(a) Isothermal relaxation solutions (pure MD and a new DSMC model).⁵³

(b) Rotational collision number determined by MD isothermal relaxation simulations.⁵⁷ Line colors represent: $T_{inf} = 100$ (black), 300 (blue), 1000 (green), and 2000 (red) degrees Kelvin.

Figure 8: Dependence of the rotational collision number on the direction to, and magnitude from, the equilibrium state as calculated by Molecular Dynamics.

Current work focuses on vibrational nonequilibrium and rotation-vibration coupling. The noble gas studies and the rotational study in nitrogen (where vibration was not excited) used simple Lennard-Jones potentials whose accuracy is rather well established for the species interactions and energies considered above. However, for vibrational relaxation at high energies, the accuracy of MD calculations becomes more sensitive to the PES where, in particular, the shape of the ‘repulsive wall’ becomes important. A large number of vibrational relaxation calculations have been performed using pure MD over a wide temperature range where the vibrational relaxation time constant (τ_v) was extracted and compared to the experimental correlation from Millikan and White⁴⁹ as well as high-temperature corrections from Park⁶² and Haas and Boyd.⁶³ The results are shown in Fig. 9a where a Quasi-Classical-Trajectory (QCT) result from Billing and Fisher⁶⁴ is also included in the low temperature range. As can be seen in Fig. 9a, there is more than an order of magnitude discrepancy when using a LJ potential with a power law exponent of 12 versus using the Ling-Rigby Harmonic Oscillator (HO) potential⁶⁵ which has a more realistic exponential fit for the repulsive wall leading to close agreement with experiment and QCT results of Billing and Fisher. A preliminary all-atom MD solution for a nitrogen shock wave including rotational and vibrational excitation with the Ling-Rigby potential is shown in Fig. 9b to qualitatively agree with a solution from DSMC. For this preliminary result, the free-stream temperature was elevated to a high value of 2500 K for the purpose of shortening the shock thickness (increasing the vibrational excitation rate) and therefore requiring less computational resources for the MD calculation. The MD simulation, which requires only PES as input, produces a low scatter solution that clearly exhibits the expected trend of rotational energy equilibrating quickly with translational energy followed by vibrational energy equilibrating with both translation and rotation. The MD simulation produces a large amount of data, including velocity and energy distribution functions throughout the shock wave that can be compared to DSMC simulations which employ rotational and vibrational collision numbers as well as the Borgnakke-Larsen energy redistribution model. Research is now focused on high temperature

conditions where rotational and vibrational relaxation is not as clearly decoupled, situations where rotational energy may equilibrate with vibrational energy prior to equilibrating with translational energy, and further investigating rotational-vibrational coupling to dissociation chemistry.

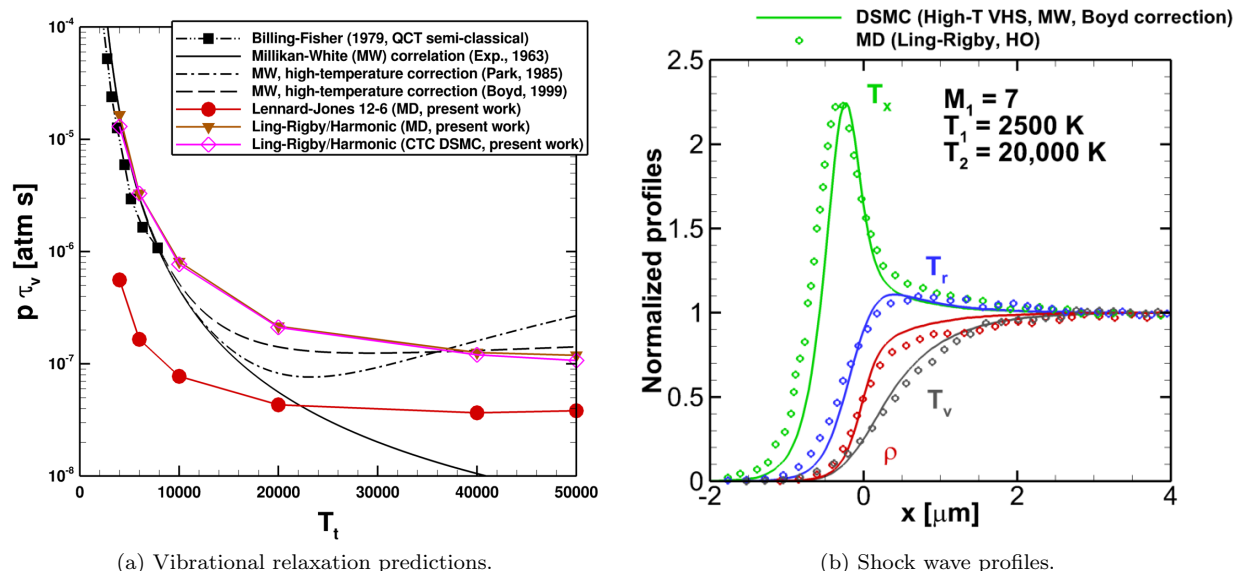


Figure 9: Molecular Dynamics predictions for vibrational relaxation and shock wave profiles including vibrational excitation in nitrogen.

Finally, it is possible to imbed molecular dynamics trajectories directly into DSMC simulations. In this manner, the rigorous simplifications employed by DSMC are maintained; using simulator particles that each represent a large number of identical real molecules, moving simulator particles with timesteps on the order of τ_c , and stochastically selecting collision pairs and initial orientations within volumes (computational cells) on the order of λ . However, the collision *models* in DSMC are completely replaced by trajectory calculations performed on arbitrary PES. This technique was introduced by Koura in 2001 as Classical-Trajectory-Calculation (CTC) DSMC^{66–68} where trajectories were combined with the null-collision DSMC algorithm. In another series of conference publications, Fujita et al. combine the VHS collision model with Quasi-Classical-Trajectories (QCT) to first study rotational/vibrational excitation and dissociation of nitrogen^{69,70} and later the dissociation of carbon monoxide through collisions with atomic oxygen.⁷¹ However, combining a collision rate dictated by a phenomenological model such as VHS with QCT analysis for reaction cross-sections can lead to unphysical reaction probabilities, especially when the VHS model is extrapolated and used at high temperatures.⁷² It is desirable for CTC-DSMC and QCT-DSMC simulations to be dependent only on the specification of a PES and not on any other phenomenological collision model.

Recently, a CTC-DSMC implementation that uses the NTC scheme with a cross-section that is determined by the PES and is consistently applied as the maximum impact parameter for the trajectory calculations was developed by Norman, Valentini, and Schwartzentruber.⁷³ Since both DSMC-CTC and pure MD simulations can use the same PES as the only model input, the two particle simulation techniques can now be directly compared. For example, Fig. 10 compares CTC-DSMC and pure MD solutions for a $M_1 = 7$, $T_1 = 28.3$ K, $\rho_1 = 0.1$ kg/m³ diatomic nitrogen shock. A comparison between normalized density and temperature profiles is shown in Fig 10(a). The rotational energy distribution functions at different values of the normalized T_{rot} in the shock are shown in Fig 10(b). Rotational energies are binned to the nearest value of $j/10$, where j is the rotational quantum number for rigid rotor molecular nitrogen with a bond length of 1.094 Å. All of the rotational distribution functions are normalized. The results of CTC-DSMC and MD simulations are in perfect agreement.

The MD density and rotational temperature profiles and rotational distribution functions shown in Fig. 10 have been previously validated with experimental data.⁵⁷ It is noted that no DSMC collision model exists that is able to exactly reproduce the MD results to this level of precision.^{53,57} Thus for the flows considered (and potentially for more complex flows), CTC-DSMC is shown to be purely a numerical acceleration technique

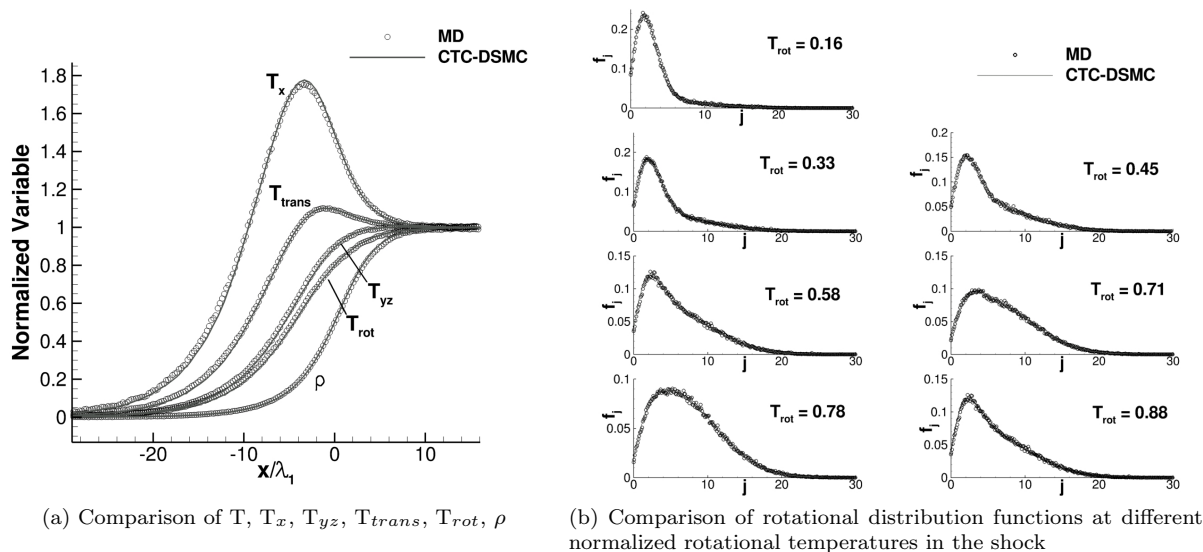


Figure 10: Comparison of CTC-DSMC to MD for $M_1 = 7$, $T_1 = 28.3$ K, $\rho_{01} = 0.1$ kg/m³.

for the MD simulation of dilute gases, since both methods require only the PES as a model input.

One important topic recently considered in CTC-DSMC simulations is three body collisions.⁷⁴ In general, two body collisions may take an arbitrary length of time and have a finite probability of colliding with third atom/molecule during a DSMC timestep, which is defined as a three body collision. Such physics, naturally captured by pure MD simulations, are not explicitly modeled by either the DSMC or CTC-DSMC methods without additional considerations. One of the difficulties associated with implementing three body collisions in a DSMC code is a description of the life-time and collision cross-section of pseudo-particles (two body collisions that have not yet completed), which are ill-defined for typical DSMC collision models.⁷⁵ In CTC-DSMC simulations we can readily calculate both of these values, enabling an unambiguous description of the three body collision rate (Z_{3B}). Additionally, the results of CTC-DSMC simulations can be directly compared to pure MD simulations with an identical interatomic potential, ensuring a rigorous validation of the three body collision algorithm. If CTC-DSMC simulations including three body collisions can be successfully validated with pure MD, this would enable the simulation of 2D and even 3D flows over complex geometries including dissociation/recombination chemistry with only a set of PES (governing individual trajectory calculations) as input.

Although much more efficient than pure MD simulation (simulating every real atom with femtosecond timescales), CTC-DSMC remains roughly 2 to 3 orders of magnitude more computationally expensive than standard DSMC, depending on the complexity of the PES used for the trajectories. However, CTC-DSMC calculations have been shown to scale extremely well on parallel architectures (including GPU architectures⁷³). Essentially, the CTC-DSMC technique automates the generation of state-to-state transition rate data, which is discussed in the next section. Instead of performing billions of *independent* trajectories to determine state-transition probabilities, the billions of trajectories are imbedded within an actual flow simulation. In this manner, the trajectories performed within a CTC-DSMC simulation are naturally those that are most relevant to the problem being simulated. The influence of specific PES can immediately be determined and variations in PES (which model the same species interactions to different accuracy) can be directly compared for full flow fields without the need to generate and converge full state-to-state cross-section models and implement in a DSMC code for each variation of a PES. Thus, CTC-DSMC may be useful in guiding the development of state-to-state models and lead to insight into physical-based model reduction strategies. However, once a consensus is established on the accuracy of a PES for a specific species interaction and state-to-state transition probabilities are converged, then a state-resolved DSMC technique could be directly validated against CTC-DSMC solutions and would then be superior to CTC-DSMC in terms of computational efficiency.

V. State-Resolved DSMC Simulations

Since DSMC simulator particles are representative of a large number of identical real molecules, they contain real molecular properties such as velocity, species type, and rotational/vibrational internal energies (either classical or quantum states). In principle, it is possible to specify quantum state-to-state transition probabilities to replace phenomenological collision models in DSMC. Large look-up tables could be utilized to incorporate these probabilities into a DSMC simulation, which may not increase the computational requirements of DSMC at all. In fact, it is possible that such look-up tables *reduce* the computational requirements, although this remains to be evaluated.

For nitrogen there are 9,390 rotational and vibrational states in the electronic ground state. The maximum vibrational state is 60 and the maximum rotational state is variable for each vibration level ranging from 2 to 279. Scientists at NASA Ames Research Center recently constructed a PES for $N+N_2$ collisions^{76,77} involving 23 million reaction cross-sections. These were used by Panesi et al.⁷⁸ to form thermally averaged rates for CFD. However, the individual cross sections can be directly used in DSMC for highly non-equilibrium flows (non-Boltzmann energy distributions). Indeed, this data was recently used by Kim and Boyd to perform state-resolved DSMC simulations.⁷⁹ The general methodology and key issues involved in constructing and implementing a state to state model are summarized from Ref. 79 here.

Before applying a specific state-transition probability to a collision pair in a DSMC simulation, the number of collision pairs selected per unit time per volume (the collision rate) must be specified. This is typically achieved through the use of a total collision cross section. The total collision cross-section can be expressed classically as the product of a geometric cross section πb_{max}^2 and an averaged probability of collision $P(E_{tr})$, as:

$$\sigma_T(E_{tr}) = 2\pi \int b db = \pi b_{max}^2 P(E_{tr}) , \quad (2)$$

$$P(E_{tr}) = \frac{1}{(2\pi)^3 b_{max}^2} \int_{b=0}^{b_{max}} \int_{\theta=0}^{\pi} \int_{\phi=0}^{2\pi} p(E_{tr}, b, \theta, \phi) b \sin\theta db d\theta d\phi , \quad (3)$$

where $p(E_{tr}, b, \theta, \phi)$ is a trajectory-computed probability that the collision occurs (as b varies from 0 to b_{max}). Equations 2 and 3 are valid for atom-atom collisions. For atom-molecule collisions, these equations are extended as follows:

$$\sigma_T(E_{tr}) = 2\pi \int b db = \pi b_{max}^2 P(E_{tr}, v, J) , \quad (4)$$

$$P(E_{tr}, v, J) = \frac{1}{(2\pi)^3 b_{max}^2} \int_{b=0}^{b_{max}} \int_{\theta=0}^{\pi} \int_{\phi=0}^{2\pi} \int_{R=\rho^-}^{\rho^+} \int_{\eta=0}^{2\pi} p(E_{tr}, b, \theta, \phi, R, \eta) b \sin\theta db d\theta d\phi dR(v, J) d\eta(J) , \quad (5)$$

where the internuclear distance R is a dependent variable of the vibrational and rotational state (v, J) and the initial orientation of the angular momentum of the molecule η is dependent on the rotational state J . In this manner, the total cross section is dependent on the rotational and vibrational states of the molecule. Thus for N_2 we need 9390 sets of total cross-sections for each relative translational energy. However, as seen in Fig. 11, the total cross-section does not strongly depend on the rotational quantum level, but mainly on the vibrational level. Kim and Boyd, thus reduced the total cross-sections to 61 and parameterized them as $\sigma_T(E_{tr}, v) = f(\mathbf{a}_v, E_{tr})$, where \mathbf{a}_v are curve-fit coefficients specific to a vibrational state v . It is interesting to note in Fig. 11 that the total cross-section predicted by the STS model is roughly 5 to 6 times larger than predicted by VSS and VHS models even at low relative energies. This implies that the simulated viscosity of these models differs substantially. The rotational and vibrational relaxation numbers determined by the STS model are shown in Fig. 12 where, notably, the rotational and vibrational relaxation numbers approach the same value in the high temperature limit.

Thus, in a DSMC simulation, a selected pair can be collided with a probability proportional to the total cross-section calculated via the above equations, which are functions not only of the relative translational energy of the selected pair, but also of the vibrational level if one is a molecule. The above can readily be extended to molecule-molecule collisions if an accurate trajectory database exists. Subsequently, for each pair determined to collide, the post collision state can be selected through the use of tabulated bound-bound and bound-free transition probabilities (determined via quasi classical trajectory simulations). For atom-molecule collisions, the state-to-state transition probabilities were determined as:

$$P_b(E_{tr}; v, J \rightarrow v' J') = \int_{v_0}^{v'} dv'' \int_{J_0}^{J'} dJ'' \frac{\sigma_b(E_{tr}; v, J \rightarrow v'', J'')}{\sigma_T(E_{tr}, v, J)} . \quad (6)$$

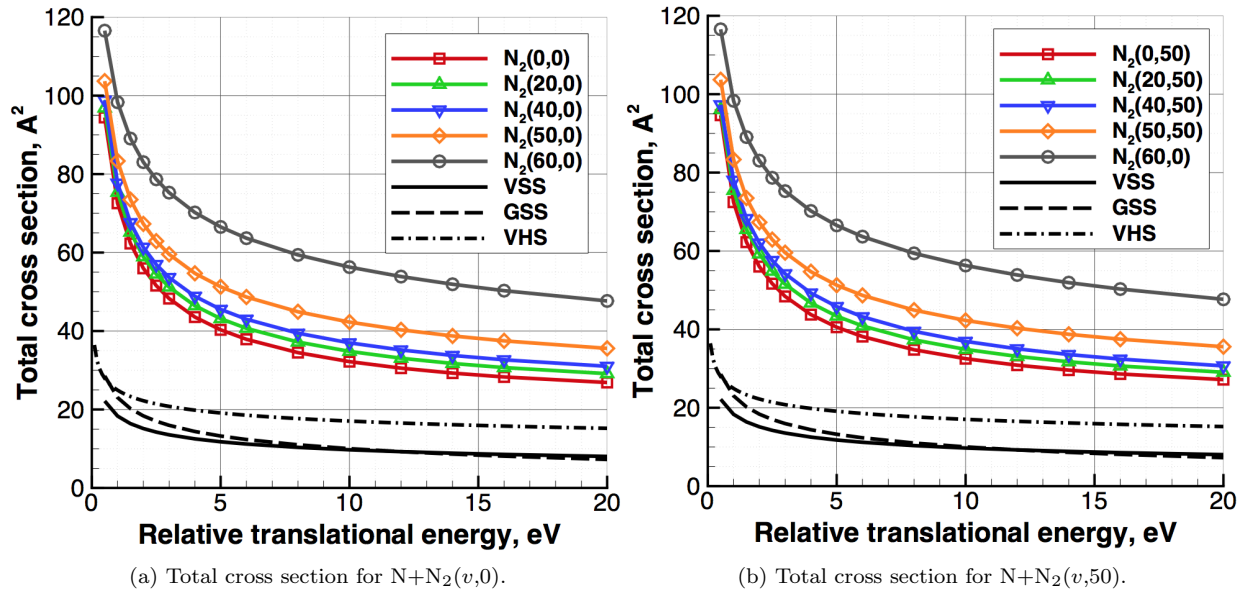


Figure 11: Total cross-sections calculated from the STS model and typical DSMC models.⁷⁹

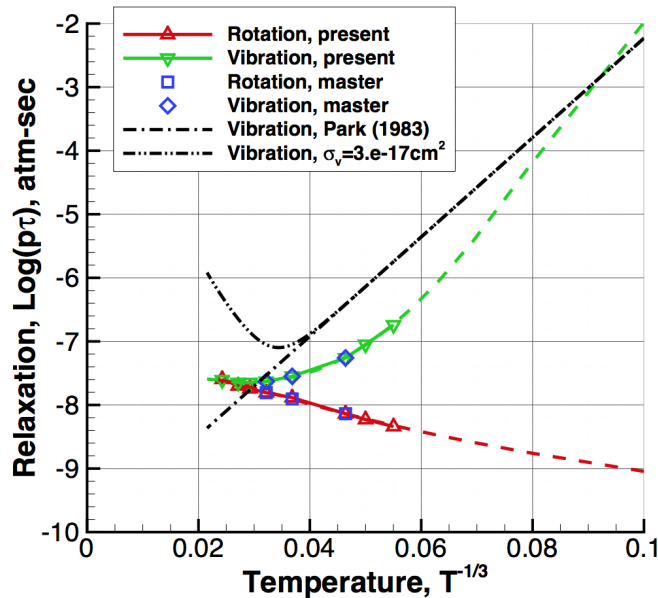


Figure 12: Rotational and vibrational relaxation parameters of $\text{N} + \text{N}_2$.⁷⁹

One key aspect is whether or not to impose microscopic reversibility. In the work of Ref. 79, microscopic reversibility is adopted in the state-to-state cross-sections as:

$$\sigma(E_{tr}; v, J \rightarrow v', J') (2J+1) g_s m_r E_{tr} = \sigma(E_{tr}; v', J' \rightarrow v, J) (2J'+1) g'_s m_r E'_{tr}, \quad (7)$$

where for N_2 , the nuclear spin degeneracy, g_s , is 6 when J is even and 3 when J is an odd number. The bound free transitions (reaction probabilities) are determined as:

$$P_f(E_{tr}; v, J \rightarrow c) = \frac{\sigma_f(E_{tr}; v, J \rightarrow c)}{\sigma_T(E_{tr}, v, J)}. \quad (8)$$

The cross-sections σ_b and σ_f were obtained from the NASA trajectory database for N+N₂.

Another state-to-state model recently implemented in DSMC involves the vibrational transition rate coefficients based on the forced harmonic oscillator (FHO) approach developed by Adamovich et al.⁸⁰ The rate coefficients are obtained through thermal averaging of collision based transition probabilities. The rate coefficient expressions are developed separately for VT and VV transitions. For VT transitions, in a molecule-molecule collision, the probability of transition from initial vibrational level (i) to final vibrational level (f) is given by

$$P_{VT}(i \rightarrow f, \epsilon) = i!f! \epsilon^{i+f} \exp(-\epsilon) \left| \frac{(-1)^r}{r!(i-r)!(f-r)! \epsilon^r} \right|^2, \quad (9)$$

$$\epsilon = S_{VT} \frac{4\pi^3 \omega (m^2/\mu) \gamma^2}{\alpha^2 h} \sinh^{-2} \left(\frac{\pi \omega}{\alpha v} \right). \quad (10)$$

In these equations, S_{VT} is a steric factor, ω is the oscillator frequency, m is the collision reduced mass, μ is the oscillator reduced mass, γ is oscillator mass ratio, α characterizes the intermolecular potential, h is Planck's constant, and v is the symmetrized relative velocity. The studies of Adamovich et al. show that these models provide rate coefficients for nitrogen that are in good agreement with values obtained by Billing and Fisher using a quantum classical model.

VT transitions using the FHO model were implemented in DSMC in Refs. 81 and 82. Boyd and Josyula⁸³ recently extended the implementation to include full VVT transitions. The model was verified to produce expected rate coefficients, and was partly validated through its application to a Mach 7 shock wave for which experimental measurements of the vibrational levels of carbon monoxide exist in the literature. Future work will aim to extend the DSMC-FHO model to include the effects of molecular dissociation.

A subtle issue that arises when implementing a state-to-state model derived from rate expressions (such as the DSMC-FHO model) is that information regarding the total cross-section is missing. A typical DSMC model (such as VHS) could be used to determine the collision rate and the probabilities in Eq. 9 applied to selected pairs.⁸² However, combining a collision rate dictated by a phenomenological model with state-to-state analysis for reaction cross-sections can lead to unphysical reaction probabilities, especially when the phenomenological model is extrapolated and used at high temperatures.⁷² Also, if a total cross-section model is imposed (an imposed viscosity model), then there will be an inconsistency in using transition *rates* to determine/implement transition *probabilities* that are applied to pairs already selected for a collision. This inconsistency is likely to cause issues with the DSMC simulation satisfying detailed balance. Detailed balance could be enforced (for a specified total cross-section model) by adjusting the transition probabilities, however, the required adjustment should be verified to be small, so as to maintain the specified transition probabilities.

Thus, a state-to-state model based on an ab-initio trajectory database can lead to consistent total cross-sections and transition probabilities. Other methods of developing state-to-state models (such as the FHO model) are promising as well, provided that any associated inconsistencies can be resolved.

VI. Summary

The direct simulation Monte Carlo (DSMC) method takes advantage of three inherent properties of dilute gases by using simulator particles that each represent a large number of identical real molecules, moving simulator particles with timesteps on the order of τ_c , and stochastically selecting collision pairs and initial orientations within volumes (computational cells) on the order of λ . These are rigorous simplifications based on sound physical principles. Historically, DSMC methods also use probabilistic rules to determine the local collision rate and collision outcomes, thus introducing collision *models*. However, new research may incorporate classical or quasi-classical trajectory calculations within DSMC and ultimately seek to use state-to-state transition probabilities; essentially replacing phenomenological collision models with ab-initio derived information. DSMC simulator particles represent real molecules with quantized internal energy levels and, thus, the method is inherently constructed to incorporate such advanced collision models and has the potential to connect the fields of computational chemistry with aerothermodynamics.

Advances in numerical modeling must be validated by experimental data, which is very difficult to obtain for hypersonic flows in thermochemical nonequilibrium. Three experiments that have directly led to validated modeling improvements for the DSMC method in recent years included: an experimental campaign at the LENS facility focused on viscous interactions on slender bodies, the BSUV-2 flight experiment which obtained

spectra (for NO) within the shock layer, and the RAM-C flight experiment that provided plasma density measurements surrounding the vehicle upon re-entry.

Strategies to improve computational efficiency generally involve local time-stepping and selecting nearest-neighbor particles for collision pairs in order to reduce the mean-collision-separation while possibly increasing the overall cell size and thus reducing the number of simulation particles. These techniques have been demonstrated as effective in many cases, however, no general consensus on the accuracy and most optimal procedures exists. Ultimately, in order to completely overlap with continuum flows over complex 3D geometries, a hybrid particle-continuum strategy is required. This capability has progressed significantly over the past decade and can now be applied to flows in strong translational-rotational-vibrational nonequilibrium. Current research is focused on multi-species flows and chemically reacting flows. For such capability to be realized, the physical models must be highly consistent between particle and continuum methods. In many cases, a molecular-based model simply can not integrate to match the functional form of a continuum based model that is a curve fit to experimental data. As a result, new thermochemical models may need to be developed that are mathematically consistent at both the molecular and continuum level and are also consistent with experimental data.

All-atom Molecular Dynamics simulations of nonequilibrium flow features (such as shock waves) are now possible. Such calculations are able to verify the underlying assumptions of the DSMC method and also trajectory-based-DSMC methods, through direct comparison using the same input Potential Energy Surface. MD simulations have led to new insights in how to model the dependence of the rotational relaxation rate on the direction to the equilibrium state, including the development of a new DSMC model. MD research now focuses on vibrational nonequilibrium, rotation-vibration coupling, and internal energy coupling to dissociation.

Finally, state-to-state models hold great promise for the DSMC method, which inherently contains the framework to implement such models in a numerically efficient manner. Precise implementations of state-to-state models still involve subtle issues (such as detailed balance) that need to be resolved. However, the main challenges involve the creation of full ab-initio trajectory databases, state-resolved model reductions that maintain accuracy, and generating high quality experimental data.

VII. Acknowledgements

TES gratefully acknowledges support from the Air Force Office of Scientific Research Young Investigator Program (YIP) Grant FA9550-10-1-0075. IDB gratefully acknowledges funding for this work through Air Force Office of Scientific Research Grants FA9550-11-1-0309 and FA9550-12-1-0483. The views and conclusions contained herein are those of the authors and should not be interpreted as necessarily representing the official policies or endorsements, either expressed or implied, of the AFOSR or the U.S. Government.

REFERENCES

- ¹Bird, G. A., "Approach to Translational Equilibrium in a Rigid Sphere Gas," *Physics of Fluids*, Vol. 6, 1963, pp. 1518–1519.
- ²Bird, G. A., *Molecular Gas Dynamics*, Oxford University Press, Oxford, UK, 1976.
- ³Bird, G. A., *Molecular Gas Dynamics and the Direct Simulation of Gas Flows*, Oxford University Press, Oxford, UK, 1994.
- ⁴Vincenti, W. and Kruger, C., *Introduction to Physical Gas Dynamics*, Robert E. Kreiger Publishing Company, Malabar, Florida, 1965.
- ⁵Gallis, M. A., Boyles, K. A., and LeBeau, G. J., "DSMC Simulations in Support of the STS 107 Accident Investigation," *AIP Conference Proceedings*, Vol. 762, pp. 1211–1216.
- ⁶Chavis, Z. and Wilmoth, R. G., "Plume Modeling and Application to Mars 2001 Odyssey Aerobraking," *Journal of Spacecraft and Rockets*, Vol. 42, No. 3, 2005, pp. 450–456.
- ⁷Wilmoth, R. G., Mitcheltree, R. A., and Moss, J. N., "Low-Density Aerodynamics of the Stardust Sample Return Capsule," *Journal of Spacecraft and Rockets*, Vol. 36, No. 3, 1999, pp. 436–441.
- ⁸Zhong, J., Ozawa, T., and Levin, D. A., "Modeling of Stardust Reentry Ablation Flows in the Near-Continuum Flight Regime," *AIAA Journal*, Vol. 46, No. 10, 2008, pp. 2568–2581.
- ⁹Boyd, I. D., Trumble, K. A., and Wright, M. J., "Modeling of Stardust Entry at High Altitude, Part 1: Flowfield Analysis," *Journal of Spacecraft and Rockets*, Vol. 47, No. 5, 2010, pp. 708–717.
- ¹⁰Boyd, I. D. and Jenniskens, P. M., "Modeling of Stardust Entry at High Altitude, Part 2: Radiation Analysis," *Journal of Spacecraft and Rockets*, Vol. 47, No. 6, 2010, pp. 901–909.
- ¹¹Holden, M. and Wadhams, T., "Code Validation Study of Laminar Shock/Boundary layer and Shock/Shock Interactions in Hypersonic Flow. Part A: Experimental Measurements," 2001, AIAA Paper 2001-1031.
- ¹²Erdman, P., Zipf, E., Espy, P., Howlett, L., Levin, D., Collins, R., and Candler, G., "Measurements of Ultraviolet Radiation From a 5 km/sec Bow Shock," *Journal of Thermophysics and Heat Transfer*, Vol. 8, 1994, pp. 441–446.

- ¹³Moss, J. and Bird, G., "Direct Simulation Monte Carlo Simulations of Hypersonic Flows With Shock Interactions," *AIAA Journal*, Vol. 43, 2005, pp. 2565–2573.
- ¹⁴Levin, D., Candler, G., Collins, R., Erdman, P., Zipf, E., and Howlett, L., "Examination of Ultraviolet Radiation Theory for Bow Shock Rocket Experiments-I," *Journal of Thermophysics and Heat Transfer*, Vol. 8, 1994, pp. 447–453.
- ¹⁵Levin, D., Candler, G., Howlett, L., and E.E., W., "Comparison of Theory With Atomic Oxygen 130.4 nm Radiation Data From the Bow Shock Ultraviolet 2 Rocket Flight," *Journal of Thermophysics and Heat Transfer*, Vol. 9, 1995, pp. 629–635.
- ¹⁶Candler, G., Boyd, I., and Levin, D., "Continuum and DSMC Analysis of Bow Shock Flight Experiments," 1993, AIAA Paper 1993-0275.
- ¹⁷Boyd, I., Bose, D., and Candler, G., "Monte Carlo Modeling of Nitric Oxide Formation Based on Quasi-Classical Trajectory Calculations," *Physics of Fluids*, Vol. 9, 1997, pp. 1162–1170.
- ¹⁸Whiting, E., Park, C., Liu, Y., Arnold, J., and Paterson, J., *NEQAIR96, Nonequilibrium and Equilibrium Radiative Transport and Spectra Program: User's Manual*, NASA Reference Publication 1389, 1996.
- ¹⁹Boyd, I., Candler, G., and Levin, D., "Dissociation Modeling in Low Density Hypersonic Flows of Air," *Physics of Fluids*, Vol. 7, 1995, pp. 1757–1763.
- ²⁰Boyd, I., Phillips, W., and Levin, D., "Sensitivity Studies for Prediction of Ultra-Violet Radiation in Nonequilibrium Hypersonic Bow-Shock Waves," *Journal of Thermophysics and Heat Transfer*, Vol. 12, 1998, pp. 38–44.
- ²¹Grantham, W., *Flight Results of a 25000 Foot Per Second Reentry Experiment Using Microwave Reflectometers to Measure Plasma Electron Density and Standoff Distance*, NASA Technical Note D-6062, 1970.
- ²²Linwood-Jones, W. and Cross, A., *Electrostatic Probe Measurements of Plasma Parameters for Two Reentry Flight Experiments at 25000 Feet Per Second*, NASA Technical Note D-6617, 1972.
- ²³Boyd, I., "Modeling of Associative Ionization Reactions in Hypersonic Rarefied Flows," *Physics of Fluids*, Vol. 19, 2007, pp. 096102.
- ²⁴Kannenber, K. C. and Boyd, I., "Strategies for Efficient Particle Resolution in the Direct Simulation Monte Carlo Method," *Journal of Computational Physics*, Vol. 157, 2000, pp. 727–745.
- ²⁵LeBeau, G., Boyles, K., and Lumpkin, F., "Virtual sub-cells for the direct simulation Monte Carlo method," 2003, AIAA Paper 2003-1031.
- ²⁶Bird, G., "Visual DSMC program for two-dimensional and axially symmetric flows," 2006, The DS2V Program Users Guide, Version 3.8, GAB Consulting.
- ²⁷Burt, J. M., Josyula, E., and Boyd, I., "Novel Cartesian Implementation of the Direct Simulation Monte Carlo Method," *Journal of Thermophysics and Heat Transfer*, Vol. 26, No. 2, 2012, pp. 258–270.
- ²⁸Bird, G., "The DS2V/3V program suite for DSMC calculations," *AIP Conference Proceedings*, Vol. 762, pp. 541–546.
- ²⁹Gallis, M., Torczynski, J., Rader, D., and Bird, G., "Convergence behavior of a new DSMC algorithm," *Journal of Computational Physics*, Vol. 228, 2009, pp. 4532–4548.
- ³⁰Hash, D. B. and Hassan, H. A., "Assessment of Schemes for Coupling Monte Carlo and Navier-Stokes Solution Methods," *Journal of Thermophysics and Heat Transfer*, Vol. 10, No. 2, 1996, pp. 242–249.
- ³¹Hash, D. B. and Hassan, H. A., "A Decoupled DSMC/Navier-Stokes Analysis of a Transitional Flow Experiment," *AIAA Paper 96-0353*, Jan. 1996, presented at the 34th AIAA Aerospace Sciences Meeting and Exhibit, Reno, NV.
- ³²Roveda, R., Goldstein, D. B., and Varghese, P. L., "Hybrid Euler/Particle Approach for Continuum/Rarefied Flows," *Journal of Spacecraft and Rockets*, Vol. 35, No. 3, 1998, pp. 258–265.
- ³³Roveda, R., Goldstein, D. B., and Varghese, P. L., "Hybrid Euler/Direct Simulation Monte Carlo Calculation of Unsteady Slit Flow," *Journal of Spacecraft and Rockets*, Vol. 37, No. 6, 2000, pp. 753–760.
- ³⁴Wang, W. L. and Boyd, I. D., "Hybrid DSMC-CFD Simulations of Hypersonic Flow over Sharp and Blunted Bodies," *AIAA Paper 03-3644*, 2003, presented at the 36th AIAA Thermophysics Conference, Orlando, FL.
- ³⁵Wijesinghe, H. S., Hornung, R. D., Garcia, A. L., and Hadjiconstantinou, N. G., "Three-dimensional Hybrid Continuum-Atomistic Simulations For Multiscale Hydrodynamics," *Journal of Fluids Engineering*, Vol. 126, 2004, pp. 768–777.
- ³⁶Schwartzentruber, T. E., Scalabrin, L., and Boyd, I. D., "A Modular Particle-Continuum Numerical Method for Hypersonic Nonequilibrium Gas Flows," *Journal of Computational Physics*, Vol. 225, No. 1, 2007, pp. 1159–1174.
- ³⁷Burt, J. M. and Boyd, I. D., "A hybrid particle approach for continuum and rarefied flow simulation," *Journal of Computational Physics*, Vol. 228, 2009, pp. 460–475.
- ³⁸Schwartzentruber, T. E. and Boyd, I. D., "A hybrid particle-continuum method applied to shock waves," *Journal of Computational Physics*, Vol. 215, No. 1, 2006, pp. 402–416.
- ³⁹Schwartzentruber, T. E., Scalabrin, L. C., and Boyd, I. D., "Hybrid Particle-Continuum Simulations of Nonequilibrium Hypersonic Blunt-Body Flowfields," *Journal of Thermophysics and Heat Transfer*, Vol. 22, No. 1, 2008, pp. 29–37.
- ⁴⁰Schwartzentruber, T. E., Scalabrin, L. C., and Boyd, I. D., "Multiscale Particle-Continuum Simulations of Hypersonic Flow over a Planetary Probe," *Journal of Spacecraft and Rockets*, Vol. 45, No. 6, 2008, pp. 1196–1206.
- ⁴¹Schwartzentruber, T. E., Scalabrin, L. C., and Boyd, I. D., "Hybrid Particle-Continuum Simulations of Hypersonic Flow over a Hollow-Cylinder-Flare Geometry," *AIAA Journal*, Vol. 46, No. 8, 2008, pp. 2086–2095.
- ⁴²Deschenes, T., Alkandry, H., and Boyd, I. D., "Application of a Modular Particle-Continuum Method to Hypersonic Propulsive Deceleration," 2011, AIAA Paper 2011-3137.
- ⁴³Deschenes, T. R., Holman, T. D., and Boyd, I. D., "Effects of Rotational Energy Relaxation in a Modular Particle-Continuum Method," *Journal of Thermophysics and Heat Transfer*, Vol. 25, No. 2, 2011, pp. 218–227.
- ⁴⁴Deschenes, T. R. and Boyd, I. D., "Extension of a Modular Particle-Continuum Method to Vibrationally Excited, Hypersonic Flows," *AIAA Journal*, Vol. 49, No. 9, 2011, pp. 1951–1959.
- ⁴⁵Verhoff, A. M. and Boyd, I. D., "Extension of a hybrid particle-continuum method for a mixture of chemical species," 2012, pp. 342–349, AIP Conf. Proc. 1501.
- ⁴⁶Schwartzentruber, T. E., Scalabrin, L. C., and Boyd, I. D., "Modular Implementation of a Hybrid DSMC-NS Solver for Hypersonic Non-Equilibrium Flows," 2007, AIAA Paper 2007-613.
- ⁴⁷Holman, T. D. and Boyd, I. D., "Effects of Continuum Breakdown on the Surface Properties of a Hypersonic Sphere," *Journal of Thermophysics and Heat Transfer*, Vol. 23, No. 4, 2009, pp. 660–673.
- ⁴⁸Sun, Q. and Boyd, I. D., "Evaluation of Macroscopic Properties in the Direct Simulation Monte Carlo Method," *Journal of Thermophysics and Heat Transfer*, Vol. 19, No. 3, 2005, pp. 329–335.
- ⁴⁹Millikan, R. C. and White, D. R., "Systematics of Vibrational Relaxation," *Journal of Chemical Physics*, Vol. 39, No. 12, 1963, pp. 3209–3213.
- ⁵⁰Lumpkin, F. E., Haas, B. L., and Iain D. Boyd, "Resolution of differences between collision number definitions in particle

- and continuum simulations," *Physics of Fluids A*, Vol. 3, No. 9, 1991, pp. 2282–2284.
- ⁵¹Haas, B. L., Hash, D. B., Bird, G. A., Lumpkin, F. E., and Hassan, H. A., "Rates of thermal relaxation in direct simulation Monte Carlo methods," *Physics of Fluids*, Vol. 6, No. 6, 1994, pp. 2191–2201.
- ⁵²Wysong, I. J. and Wadsworth, D. C., "Assessment of direct simulation Monte Carlo phenomenological rotational relaxation models," *Physics of Fluids*, Vol. 10, No. 11, 1998, pp. 2983–2994.
- ⁵³Zhang, C., Valentini, P., and Schwartzentruber, T. E., "A Nonequilibrium-Direction-Dependent Rotational Energy Model for use in Continuum and Stochastic Molecular Simulation," 2013, AIAA Paper 2013-1202.
- ⁵⁴Valentini, P. and Schwartzentruber, T. E., "Large-scale molecular dynamics simulations of normal shock waves in dilute argon," *Physics of Fluids*, Vol. 21, No. 6, 2009, pp. 066101.
- ⁵⁵Valentini, P. and Schwartzentruber, T. E., "A combined Event-Driven/Time-Driven molecular dynamics algorithm for the simulation of shock waves in rarefied gases," *Journal of Computational Physics*, Vol. 228, 2009, pp. 8766–8778.
- ⁵⁶Valentini, P., Tump, P. A., Zhang, C., and Schwartzentruber, T. E., "Molecular Dynamics Simulations of Shock Waves in Mixtures of Noble Gases," *Journal of Thermophysics and Heat Transfer*, Vol. 27, No. 2, 2013, pp. 226–234.
- ⁵⁷Valentini, P., Zhang, C., and Schwartzentruber, T. E., "Molecular dynamics simulation of rotational relaxation in nitrogen: Implications for rotational collision number models," *Physics of Fluids*, Vol. 24, No. 10, 2012, pp. 106101.
- ⁵⁸Harnett, L. N. and Muntz, E. P., "Experimental Investigation of Normal Shock Wave Velocity Distribution Functions in Mixtures of Argon and Helium," *Physics of Fluids*, Vol. 15, No. 4, 1972, pp. 565–572.
- ⁵⁹Gmurczyk, A. S., Tarczynski, M., and Walenta, Z. A., "Shock Wave Structure in the Binary Mixtures of Gases with Disparate Molecular Masses," 1979, 11th International symposium on rarefied gas dynamics, edited by Campargue, R., Commissariat à l'Énergie Atomique, Paris.
- ⁶⁰Robben, F. and Talbot, L., "Experimental study of the rotational distribution function of nitrogen in a shock wave," *Physics of Fluids*, Vol. 9, No. 4, 1966, pp. 653–662.
- ⁶¹Parker, J. G., "Rotational and Vibrational Relaxation in Diatomic Gases," *Physics of Fluids*, Vol. 2, No. 4, 1959, pp. 449–462.
- ⁶²Park, C., "Review of chemical-kinetic problems of future NASA missions, I: Earth entries," *Journal of Thermophysics and Heat Transfer*, Vol. 7, No. 3, 1993, pp. 385–398.
- ⁶³Haas, B. L. and Boyd, I. D., "Models for direct Monte Carlo simulation of coupled vibration-dissociation," *Physics of Fluids A*, Vol. 5, 1993, pp. 478.
- ⁶⁴Billing, G. D. and Fisher, E. R., "VV and VT rate coefficients in N₂ by a quantum-classical model," *Chem. Phys.*, Vol. 43, No. 3, 1979, pp. 395–401.
- ⁶⁵Ling, M. S. H. and Rigby, M., "Towards an intermolecular potential for nitrogen," *Mol. Phys.*, Vol. 51, No. 4, 1984, pp. 855–882.
- ⁶⁶Koura, K., "Monte Carlo direct simulation of rotational relaxation of nitrogen through high total temperature shock waves using classical trajectory calculations," *Physics of Fluids*, , No. 10, pp. 2689–2691.
- ⁶⁷Koura, K., "Monte Carlo direct (test-particle) simulation of rotational and vibrational relaxation and dissociation of diatomic molecules using classical trajectory calculations," *AIP Conference Proceedings*, Vol. 585, 2001.
- ⁶⁸Koura, K., "Direct simulation Monte Carlo study of rotational nonequilibrium in shock wave and spherical expansion of nitrogen using classical trajectory calculations," *Physics of Fluids*, Vol. 14, No. 5, 2002, pp. 1689–1695.
- ⁶⁹Fujita, K., "Coupled Rotation-Vibration-Dissociation Kinetics of Nitrogen using QCT Models," 36th AIAA Thermophysics Conference, Orlando, FL, 2003, AIAA-2003-3779.
- ⁷⁰Fujita, K., "Assessment of Molecular Internal Relaxation and Dissociation by DSMC-QTC Analysis," 37th AIAA Fluid Dynamics Conference and Exhibit, Miami, FL, 2007, AIAA-2007-4345.
- ⁷¹Fujita, K., "Vibrational Relaxation and Dissociation Kinetics of CO by CO-O Collisions," 40th Thermophysics Conference, Seattle, WA, 2008, AIAA 2008-3919.
- ⁷²Deng, H., Ozawa, T., and Levin, D. A., "Analysis of Chemistry Models for DSMC Simulations of the Atmosphere of Io," *Journal of Thermophysics and Heat Transfer*, Vol. 26, No. 1, 2012, pp. 36–45.
- ⁷³Norman, P., Valentini, P., and Schwartzentruber, T. E., "GPU-accelerated Classical Trajectory Calculation Direct Simulation Monte Carlo applied to shock waves," *Journal of Computational Physics*, Vol. 247, No. 15, 2013, pp. 153–167.
- ⁷⁴Norman, P. and Schwartzentruber, T. E., "Classical Trajectory Calculation Direct Simulation Monte Carlo: GPU Acceleration and Three Body Collisions," 2013, AIAA Paper 2013-1200.
- ⁷⁵Gallis, M. A., Bond, R. B., and Torczynski, J. R., "Assesment of Reaction-Rate Predictions of a Collision-Energy Approach from Chemical Reactions in Atmospheric Flows," *AIAA 2010-4499*.
- ⁷⁶Jaffe, R., Schwenke, D., Chaban, G., and Huo, W. M., "Vibrational and Rotational Excitation and Relaxation of Nitrogen from Accurate Theoretical Calculation," 2008, AIAA Paper 2008-1208.
- ⁷⁷Jaffe, R., Schwenke, D., and Chaban, G., "Theoretical Analysis of N₂ Collisional Dissociation and Rotation-Vibration Energy Transfer," 2009, AIAA Paper 2009-1569.
- ⁷⁸Panesi, M., Jaffe, R., Schwenke, D., and Magin, T., "Rovibrational internal energy transfer and dissociation of N₂(1Σ^{g+})-N(4S_u) system in hypersonic flows," *J. Chem. Phys.*, Vol. 138, 2013, pp. 044312.
- ⁷⁹Kim, J. G. and Boyd, I. D., "State Resolved Thermochemical Modeling of Nitrogen Using DSMC," 2012, AIAA Paper 2012-2991.
- ⁸⁰Adamovich, I., Macheret, S., Rich, J., and Treanor, C., "Vibrational Energy Transfer Rates Using a Forced Harmonic Oscillator Model," *Journal of Thermophysics and Heat Transfer*, Vol. 12, 1998, pp. 57–65.
- ⁸¹Vijayakumar, P., Sun, Q., and Boyd, I., "Detailed Models of Vibrational-Translational Energy Exchange for the Direct Simulation Monte Carlo Method," *Physics of Fluids*, Vol. 11, 1999, pp. 2117–2126.
- ⁸²Li, Z., Sohn, I., and Levin, D. A., "State Specific Vibrational Relaxation and Dissociation Models for Nitrogen in Shock Wave Regions," 2012, AIAA Paper 2012-2996.
- ⁸³Boyd, I. D. and Josyula, E., "State Resolved Vibrational Relaxation Modeling for Strongly Nonequilibrium Flows," 2011, AIAA Paper 2011-0448.